PCCP

PAPER

View Article Online
View Journal

Cite this: DOI: 10.1039/d5cp05068e

Molecular insights into the effect of small molecule impurities in the ring-opening polymerization of $[PCl_2N]_3$ using quantum mechanical analysis

Yuan Xue, *[ab] Carrie R. Salmon[cd] and Valentin Gogonea[efg]

This is the first theoretical investigation that systematically analyzes the interactions between the hexachlorophosphazene, $[PCl_2N]_3$, and small molecule impurities H_2O and HCl in a 1 : 1 stoichiometric ratio. Utilizing both *ab initio* methods and seven DFT functionals in conjunction with the triple-ζ basis set, the pivotal structures in proposed reaction mechanisms are fully characterized and the energy change for each step was determined at the CCSD(T)/aTZ‖MP2/aTZ level of theory. Our QM calculations show that $[PCl_2N]_3$ can be hydrolyzed *via* a single-step mechanism with an activation energy of *ca.* 180 kJ mol^{-1}, or be ring-opened by HCl through a two-step mechanism, in which the rate-determining step has an activation energy of *ca.* 120 kJ mol^{-1}. Because the activation energy of these two reactions is notably lower than that of the ring-opening polymerization and the ring–ring expansion equilibrium (which requires *ca.* 240 kJ mol^{-1} of energy determined at a comparable DFT level of theory), our study indicates that even trace amount of H_2O and HCl can significantly interfere with the polymerization process. Beyond revealing new mechanistic details, our calculations also indicate that all selected functionals can provide reasonable electronic structures to describe the reaction progress. On the other hand, while each of the functionals investigated here excels in closely matching the CCSD(T)/aTZ‖MP2/aTZ energy barriers for certain steps in the reaction, the B3LYP functional is capable of providing the most consistent results. This establishes that the B3LYP functional can be suitable for investigating phosphazene reactions as a computationally efficient and robust quantum mechanical approach while maintaining near–*ab initio* accuracy.

Received 31st December 2025,
Accepted 14th May 2026

DOI: 10.1039/d5cp05068e

rsc.li/pccp

1. Introduction

For more than a century, polyphosphazenes have stood as a fascinating subject of study due to complicated side reactions and unexpected experimental results that seemed contradictory but diverse when using additives such as metal chlorides[1–4] or nitrogenous bases[5,6] and interacting with glassware,[7] through the catalytic activity of by-products such as $POCl_3$,[8] impurities in reagents,[9] and the presence of water.[9–14] Yet it is important to note that small molecule interactions with phosphazenes

[a] Department of Chemistry and Biochemistry, The University of Mississippi, University, MS 38677, USA. E-mail: yxue@olemiss.edu
[b] Department of Chemistry and Biochemistry, Oberlin College, Oberlin, OH 44074, USA
[c] Department of Natural & Social Sciences, State College of Florida, Manatee-Sarasota Venice Campus, Venice, FL 34293, USA
[d] Department of Physics, Kent State University, Kent, Ohio 44242, USA
[e] Department of Chemistry, Cleveland State University, Cleveland, OH 44115, USA
[f] Department of Blood, Lung, and Kidney Research, Cleveland Clinic, Cleveland, OH 44195, USA
[g] Center for Microbiome & Human Health, Cleveland Clinic, Cleveland, OH 44195, USA

Yuan Xue

Yuan Xue received his BS and PhD in Chemistry from the Rose-Hulman Institute of Technology (2016) and the University of Akron (2021), respectively. He taught at Oberlin College and Conservatory prior to his postdoctoral research under the guidance of Dr Gregory Tschumper (2022). He was recognized as one of the SEC Emerging Scholars for the academic year 2023–2024. Currently, Dr Xue serves as a faculty member at the University of Mississippi, where his research is centered on utilizing quantum mechanical calculations to investigate reaction mechanisms.

appear to play an important, yet not fully understood role in the synthesis of chlorophosphazenes.

The basic reaction to form chlorophosphazenes predominantly produces products with cyclic configuration $[PR_2N]_m$ (where R = halogens,[15–18] and the target product has m = 3) or linear species such as $–[R_2PNPR_2N]_n–$ where the unsubstituted short linear products are considered to be of minor interest. The interest in chlorophosphazenes through experimental and theoretical exploration has been documented in both comprehensive reviews[18–25] and numerous books[25–32] and has revealed a complex and interesting facet of scientific inquiry dedicated to phosphazenes and their applications.[33–53]

A significant portion of foundational phosphazene chemistry relies on $[PR_2N]_3$ which has a parent molecule where R = Cl.[18,23,25,26,54,55] Chlorophosphazenes have been the focus of scrutiny for their intriguing behavior where even the acidity of glassware is suggested as a contributing factor to their chemistry.[56] As suggested in the literature, the interaction of phosphazenes with water appears to be contradictory. While some studies report that water inhibits polymerization, others suggest a catalytic role by promoting ring-opening.[57,58] This adds complexity and a degree of uncertainty to the investigation of these compounds and the role of water.[7,12,59–61] The dual nature of their behavior, as illustrated in the reported literature, contributes to the curious yet frustrating crux of this particular field of chemistry. Although there is an experimental study that does explore the hydrolysis of phosphazene oligomers,[62] theoretical investigations of water interaction with these chlorinated compounds have not been reported in the literature yet.

Another intriguing facet of interaction of small molecules with $[PCl_2N]_3$ involves the generation of HCl,[63] a phenomenon observed during the reaction of PCl_5 with NH_4Cl in refluxing chlorobenzene.[64] This solution reaction produces both linear $–[Cl_2PNPCl_2N]_n–$ and cyclic $[PCl_2N]_m$ species, with m = 3 representing the targeted compound obtained in good yields.[9,11,26,55] Furthermore, HCl is also found in the context of melt polymerization reactions of $[PCl_2N]_m$, and it is speculated that it plays a contributing role in the formation of crosslinked polymer products.[65] Remarkably, despite its significance, this particular aspect of chlorophosphazene chemistry is yet to be thoroughly explored through computational studies. The intricate interplay between $[PCl_2N]_3$ and HCl, as well as the possible significant role that small amounts of water can play in altering the mechanistic pathway involving these materials and their polymerization reactions, remains an uncharted area in the theoretical understanding of chlorophosphazene chemistry.

Various other fundamental aspects within this field of chemistry have undergone thorough exploration through a combination of experimental[64,66] and computational[17,58,67–88] approaches. Recent advancements in the literature have shed light on the mechanistic intricacies of reactions involving chlorophosphazenes,[68,89,90] marking the initiation of the next phase in computational exploration of interaction of small molecules in these systems. Recent studies have also explored computationally other discrete areas in chlorophosphazene chemistry.[91–99] Specifically, there is a growing focus on understanding the impact of small molecules on processes inherent to chlorophosphazene reactions, thereby addressing challenges and complications that may arise during these chemical transformations and providing insights that may help find alternate pathways or mechanisms. This evolving area of research in chlorophosphazene chemistry not only builds upon the existing knowledge base but also represents a crucial step toward a more comprehensive understanding of the various factors influencing chlorophosphazene chemistry, some of which are discussed in the present study.

2. Computational methods

All electronic structures reported herein were characterized using the Gaussian16 or MolPro2022 quantum chemistry software.[100–103] To anchor the stationary points on the potential energy surface (PES), all proposed structures were fully optimized using both density functional theory (DFT) and *ab initio* methods. DFT calculations were conducted utilizing a variety of popular DFT functionals, including the Becke 3-parameter Lee–Yang–Parr hybrid functional (B3LYP)[104,105] and its variant with Becke–Johnson damping (B3LYP-D3)[106] and long-range correction (cam-B3LYP).[107] Additional functionals tested include B3PW91,[108] ωb97X-D,[109] M06-2X,[110] and PBE0.[111] All DFT calculations were conducted in conjunction with Pople's split-valence triple-ζ basis set with diffuse functions (6-311+G(d,p)) unless specified, to probe the strong non-covalent interactions between Lewis acids and $[PR_2N]_3$. On the other hand, all stationary points were also fully characterized using the *ab initio* second-order Møller–Plesset perturbation theory (MP2)[104,112–114] Hamiltonian in conjunction with Dunning's double- and triple-ζ correlation consistent basis sets augmented with diffuse functions (aug-cc-pV*X*Z, abbreviated as aXZ where X = D or T).[115,116] Frozen-core approximations were employed that excluded the 1s-like orbitals of nitrogen and oxygen, as well as the 1s-, 2s-, and 2s-like orbitals of both phosphorus and chlorine from the electron correlation calculations.

When characterizing the saddle points as transition states (TSs) on the PES, the Berny or transit-guided quasi-Newton (QST2 & QST3)[117,118] methods were employed. Harmonic vibrational frequency calculations were conducted at uniform theoretical levels to confirm the stationary points of all geometry-optimized structures. More specifically, the number of imaginary frequencies (n_i) was confirmed as 0 for all energy minima and 1 for all TSs. It should be noted that when the MP2 method is applied, Hessians were obtained analytically with the aDZ basis set but numerically with the aTZ basis set. We ensured that transition states (TS) are connected to two nearby energy minima through the intrinsic reaction coordinate (IRC) calculation.[119]

All thermodynamic properties were evaluated at 298 K and 1 atm pressure. Based on the MP2/aTZ geometry-optimized structures, two additional sets of calculations were completed.

MP2 single-point energetics were also obtained with the larger aug-cc-pVQZ (aQZ) basis set to better approach the energy barriers between stationary points near the basis set limit. Additionally, as the ''gold standard'', the coupled cluster singles, doubles, and perturbative triples (CCSD(T)) methods were applied in conjunction with the aTZ basis set to provide benchmarking energetics for the reaction pathways.[120–122]

All electronic structures are fully optimized in the gas phase. This scheme facilitated the calculation of partial atomic charges and the construction of electrostatic potential (ESP) maps,[123] offering a detailed understanding of the electrostatic distribution within the molecular framework.

In this study, all MP2 and DFT calculations with natural bond orbital (NBO) analysis were completed using the Gaussian16 program with the NBO program version 3.1.[100,124,125] The GaussView program version 6.1,[126] was employed for visualizing molecular orbitals and constructing Molecular Orbital (MO) energy level diagrams. The CCSD(T)/aTZ single point energies are completed using MolPro2022.[101–103]

The Cartesian coordinates for each stationary point characterized at different levels of theory reported herein are detailed in Tables S22–S155. The harmonic vibrational frequencies for geometries with experimental relevance are provided in Tables S7–S15.

3. Results and discussion

3.1 Reaction pathways and energetics

3.1.1 Hydrolysis of $[PCl_2N]_3$. Comprehensive QM computations suggest that the hydrolysis of $[PCl_2N]_3$ can be completed in one step. Before the reaction, the micro-hydrated $[PCl_2N]_3$ forms a hydrogen bond with a water molecule with a N–H bond length of 2.017 Å calculated at the MP2/aTZ level of theory. As the water molecule migrates towards the neighboring phosphorus atom (P), it initiates a nucleophilic attack *via* the oxygen site after overcoming an energy barrier of 173.20 kJ mol^{-1} (Table 1). The transition state (denoted as **TS** in Scheme 1) is reached when the oxygen (O) is 1.945 Å away from P. The geometrical change of the P center from a tetrahedron to a trigonal bipyramid indicates that O pushes Cl away, elongating the P–Cl bond length from 2.008 Å to 2.395 Å, and at the same time, the Cl–P–Cl bond angle is drastically increased from 101.97° to 148.91°. Such re-arrangement shifts the Cl atom to a bridging position and paves the road for an electrostatic interaction with the H atom from the water molecule. As the oxygen atom moves closer to P, the formation of the P–O bond triggers the P–Cl bond cleavage, and the ejection of Cl initiates a concerted proton transfer leading to hydrochloric acid (HCl) as a byproduct. The P-substituted hydroxyl group along with the N atom from the phosphazene ring enables the hydrolysis product, $P_3N_3Cl_5OH$, to capture the HCl byproduct *via* hydrogen bonding. Compared with the **TS**, the product with two hydrogen bonds (denoted as **P_2HB** in Scheme 1) sits 236.18 kJ mol^{-1} lower in energy than the **TS** on the potential energy surface (PES) calculated at the MP2/aTZ level of theory. The energy relaxation following the change in the hydrogen bond configurations was also thoroughly studied through both DFT and *ab initio* calculations. At the B3LYP-(D3)/6-311+G(d,p) level of theory, our results indicate that once HCl is formed, it is hydrogen-bonded to the hydroxyl group, which stabilizes the complex (forming the local minimum **P_1HB**, marked in gray in Scheme 1).

Then, after overcoming a very small energy barrier of less than *ca.* 1.5 kJ mol^{-1} (Table 1), the **P_1HB** local minimum is converted into **P_2HB** with the release of another *ca.* 16 kJ mol^{-1} of heat. Interestingly, although a similar reaction pathway can be tracked at the MP2/aDZ level of theory, the activation energy (E_a) required to reach the transition state **TS_HB** decreased to 0.01 kJ mol^{-1} (Table 1). Further investigations into anchoring the **P_1HB** on the PES utilizing the aTZ basis set were successful, and calculations indicate that the formation of a 2nd hydrogen bond can release another ~20 kJ mol^{-1} of energy. However, the vanishing energy barrier approaches zero within numerical uncertainty, indicating a barrierless hydrogen-bond rearrangement rather than a distinct kinetic step between **TS_HB** and **P_1HB** which makes it challenging to characterize this **TS** (Table 1). Based on the

Table 1 The relative energies (ΔE, in kJ mol^{-1}) of the stationary points from the hydrolysis and tautomerization catalyzed by HCl determined at different DFT levels of theory, the MP2/aXZ levels of theory where X = D, T and Q and the CCSD(T)/aTZ level of theory

	DFT								*Ab initio*			
Theory F/M[a]	B3LYP		B3LYP-D3	B3PW91	ωB97X-D	M06-2X	cam-B3LYP	PBE0	MP2			CCSD(T)
Cmpd/B[b]	aTZ	6-311+G(d,p)							aDZ	aTZ	aQZ[d]	aTZ[d]
R	0.00	0.00	0.00	0.00	0.00	0.00	0.00	0.00	0.00	0.00	0.00	0.00
TS[c]	186.84	187.42	166.96	186.11	201.28	182.70	193.57	185.76	154.40	173.20	177.33	180.99
P_1HB[c]	−34.78	−32.07	−30.05	−28.45	−30.31	−41.73	−38.89	−27.98	−24.16	−30.44	−30.53	−35.96
TS_HB	−33.73	−30.81	−28.86	−27.32	−30.28	−39.96	−37.93	−27.41	−24.15	—[e]	—	—
P_2HB	−48.76	−46.70	−48.19	−45.03	−49.16	−52.57	−55.29	−47.46	−37.99	−49.77	−49.88	−53.41
SPT_TS[c]	−33.97	−30.79	−34.46	−33.63	−31.23	−37.48	−39.56	−37.02	−21.08	−33.30	−33.75	−33.32
P	−55.20	−60.43	−61.06	−55.25	−59.43	−57.10	−67.07	−55.86	−39.82	−50.90	−50.75	−55.01

[a] Functional or method. [b] Compound and basis set. [c] Stationary points have different electronic structures at the M06-2X/6-311+G(d,p) level of theory when compared to the structures characterized at the other levels of theory. [d] Single-point energies completed based on the electronic structures fully optimized at the MP2/aTZ level of theory. [e] Not found using the computational software.

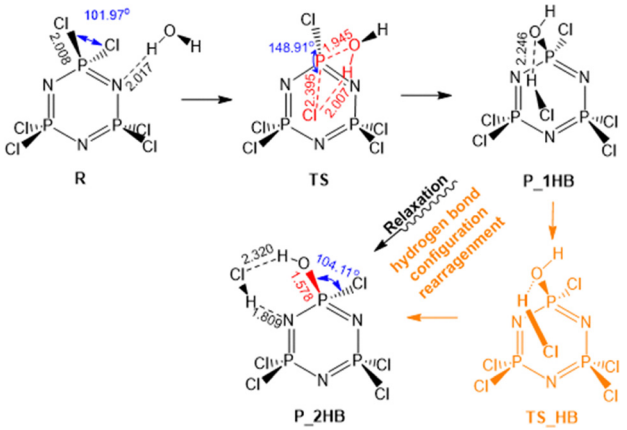

Scheme 1 The four critical stationary points anchored on the PES for the hydrolysis of $[PCl_2N]_3$ to form $P_3N_3Cl_5OH{\cdot}HCl$ calculated at the MP2/aTZ level of theory. Although the transition state associated with the hydrogen bond configuration rearrangement (**TS_HB**, colored in orange) can be identified using the DFT method and at lower levels of theory for MP2 calculations, it could not be found at the MP2/aTZ level of theory.

MP2/aTZ geometry optimized structures, further MP2 single-point calculations utilizing the larger quadruple-ζ basis set (abbreviated as MP2/aQZ‖MP2/aTZ) verified that all energy barriers determined herein differ by no more than 3% compared with the MP2/aTZ energies, although significant energy differences were noted when comparing the MP2 results with the benchmarking CCSD(T)/aTZ‖MP2/aTZ energies.

The distinct differences can be found at all minima that include intermolecular hydrogen bonding as MP2 overestimates the energy by at least 5%. On the other hand, while most DFT functionals can provide reasonable descriptions on electronic structures to probe the mechanistic pathways, it should be noted that although the M06-2X/6-311+G(d,p) level of theory can reproduce and provide reasonable energetics, major discrepancies in electronic structures were observed during the rate-determining step. More specifically, after relaxing **TS***, the local minimum **P_1HB*** contains an intermolecular hydrogen bond between HCl and an N atom from the $[PCl_2N]_3$ ring (Scheme S1). This is different from the intermolecular hydrogen bond between HCl and the hydroxyl group characterized by the calculations conducted using the MP2 method and the other DFT functionals.

Among the tested functionals, energies obtained at the B3LYP/aTZ level of theory can provide most relative energies (ΔE) within *ca.* 3.5% deviation when compared with those determined at the CCSD(T)/aTZ‖MP2/aTZ level of theory, except for **P_2HB** with a larger deviation of 8.7%. In contrast, the energies determined by using other functionals all contain at least one stationary point that has ΔE that deviates more than 10% with respect to the benchmarking CCSD(T) energies (Table S4). The deviations might be up to >20% (*e.g.* cam-B3LYP, B3PW91 and PBE0) for stationary points and >10% when determining the E_a for the rate-determining step (ωB97X-D), making them unideal as candidates for a faster and more affordable, yet still reliable QM approach for determining the energy barriers (Table S4).

To gain insight into reaction kinetics, the reaction rate constant for the rate-determining step was extrapolated using the Eyring equation. Using the activation energy determined at the CCSD(T)/aTZ‖MP2/aTZ level of theory, the rate constant for the hydrolysis is *ca.* 10^6 times larger than that of the ring-opening polymerization and the ring–ring expansion equilibrium (which requires *ca.* 240 kJ mol^{-1} of energy determined at a comparable DFT level of theory)[89] at 500 K (which is the ideal temperature for the ring-opening reaction reported in the literature). This indicates that even trace amounts of H_2O can open lower-barrier pathways and disrupt polymerization.

3.1.2 Tautomerization. The tautomerization of the hydrolyzed product was experimentally investigated and reported by Gabler and Haw in 1990,[57a] following earlier work by De Ruiter *et al.* in 1984.[57b] More recently, Allen and Hayes (2016)[57c] reported experimental studies on rearrangement reactions of phosphazenes and proposed a mechanism involving similar electrostatic mediation at the reactive site, leading to the formation of $(NPCl_2)_2P(O)NH$.[57a,b] Our computational results reflect an analogous process, resulting in the formation of **Tauto_P** (Scheme 2). Based on the previous work, the proton transfer from the hydroxyl group to the N atom was also thoroughly investigated using quantum mechanical calculations (Scheme 2). Our computations at the MP2/aTZ level of theory indicate that without the assistance or interference from any other proton source, the O–H bond is 0.968 Å before the reaction occurs. After overcoming an energy barrier of 139.01 kJ mol^{-1} (Table 2), the O–H bond elongates to 1.337 Å, bringing the proton only 1.298 Å away from N, while the P–O–H bond angle significantly decreases from 112.02° to 75.71°. Then, while the proton transfer releases *ca.* 132 kJ mol^{-1} of heat, the overall reaction is slightly endothermic (ΔH = +7.51 kJ mol^{-1}).

Further single-point calculations conducted at the MP2/aQZ and CCSD(T)/aTZ levels of theory based on the MP2/aTZ geometry-optimized structures verified that the energy barrier for the uncatalyzed tautomerization is near 140 kJ mol^{-1} and the reaction enthalpy is lower than 10 kJ mol^{-1} (Table 2). Compared with the benchmarking E_a obtained at the CCSD(T)/aTZ‖MP2/aTZ level of theory, most DFT functionals can provide accurate estimations except for B3PW91 and PBE0 as their deviations are greater than 5% (Table S5). It should be noted that at the ωB97X-D/6-311+G(d,p) level of theory, although the E_a obtained differs by no more than 0.2% when

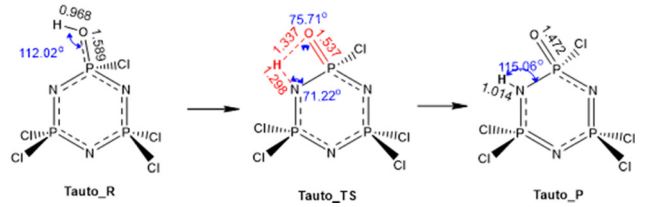

Scheme 2 The fully optimized electronic structure of the reactant, transition state and the product of the concerted step tautomerization of the hydrolyzed product of chlorophosphazene calculated at the MP2/aTZ level of theory.

Table 2 The relative energies (ΔE, in kJ mol^{-1}) of the stationary points from tautomerization without interference determined at different DFT levels of theory, the MP2/aXZ levels of theory where X = D, T and Q and the CCSD(T)/aTZ level of theory

	DFT								*Ab initio*			
Theory F/M[a]	B3LYP		B3LYP-D3	B3PW91	ωB97X-D	M06-2X	cam-B3LYP	PBE0	MP2			CCSD(T)
Cmpd/B[b]	aTZ	6-311+G(d,p)							aDZ	aTZ	aQZ[c]	aTZ[c]
Tauto_R	0.00	0.00	0.00	0.00	0.00	0.00	0.00	0.00	0.00	0.00	0.00	0.00
Tauto_TS	143.76	143.03	142.55	136.92	146.56	148.76	147.49	138.19	139.91	139.01	139.84	146.24
Tauto_P	5.23	−6.82	−10.49	−4.22	−5.19	−0.41	−3.69	−2.58	9.05	7.51	8.35	7.86

[a] Functional or method. [b] Compound and basis set. [c] Single-point energies completed based on the electronic structures fully optimized at the MP2/aTZ level of theory.

compared with the benchmarking E_a, the reaction enthalpy was significantly underestimated. In contrast, the B3LYP calculations completed using the aTZ basis set indicate that tautomerization of the hydrolyzed product is an endothermic process, which is consistent with both the MP2 and CCSD(T) results. Further investigations suggest that the thermochemistry of the reaction is sensitive to the basis set selection (Table S5). This effect becomes prominent when the stationary points include strong non-covalent interactions (*e.g.* the hydrogen bond between the O and H atoms in **Tauto_P** in Scheme 2). This is probably because the aTZ basis set offers a better description of electron correlation and polarization, providing a more balanced representation of both valence and diffuse functions, which are both crucial for accurate non-covalent interactions.

Due to the presence of trace amounts of proton sources involved in hydrolysis, other proton sources most likely interfere with the tautomerization reaction, *e.g.*, the HCl byproduct formed from the hydrolysis reaction. Starting from **P_2HB**, tautomerization can be facilitated by the double hydrogen-bonded HCl and can complete in one step *via* a synchronous proton transfer transition state (abbreviated as **SPT_TS** in Scheme 3). Requiring much less energy to initiate, the HCl-catalyzed tautomerization has an E_a of only 16.47 kJ mol^{-1} (Fig. 1 and the last three rows of Table 1) at the MP2/aTZ level of theory, a 90% decrease compared to the uncatalyzed tautomerization (Table 2). In this process, two proton transfers occur simultaneously; once the O–H bond is lengthened to 1.036 Å, the H from HCl also migrates to a bridging position 1.686 Å away from Cl and 1.162 Å from the N atom. This slightly exothermic reaction with ΔH = *ca.* −1 kJ mol^{-1} is complete when HCl is positioned to form two hydrogen bonds, one between the H of HCl and the O bound to P (1.680 Å), and the second (2.327 Å) between the Cl of HCl and the H atom bound to N. The striking difference in E_a when comparing the presence and absence of HCl highlights the catalytic properties of the acid. This result also aligns with experimental observations by Gabler and Haw,[57] who showed that the tautomerization process is highly sensitive to acidity. The formation of HCl and PClO by-products has a measurable influence on the ^{31}P NMR chemical shifts within the reaction environment. They further demonstrated that both increased acidity and the addition of bases, such as pyridine, affect the tautomerization and the subsequent hydrolysis of the chlorophosphazene ring.

Additionally, the reaction rate constant of the tautomerization reactions with and without HCl can be extrapolated based on the corresponding benchmarking activation energies using the Eyring equation. At 500 K, the tautomerization process presents a 10^{13}-fold enhancement in the presence of HCl, confirming that even trace amounts of HCl can substantially alter the kinetics.

3.1.3 Two-step $[PCl_2N]_3$ ring-opening reaction initiated by HCl. Understanding HCl-initiated ring-opening is critical because it may generate highly reactive –NH termini that promote crosslinking in polymerization reactions. As a common method to prepare $[PCl_2N]_3$ involves using PCl_5 and NH_4Cl as reactants, HCl can be generated and retained as a byproduct after synthesis. Additionally, earlier discussion from this work (see Section 3.1.1) indicates that even though $[PCl_2N]_3$ is purified, HCl can still be generated from hydrolysis with trace amounts of water. As a result, HCl can be trapped by strong non-covalent interactions (observed in **P_1HB** and **P_2HB** as discussed in Section 3.1.1) and can trigger an undesired ring-opening reaction generating a linear product with a highly reactive –NH terminal, which, eventually, gives rise to cross-linked polymers.

Our computations suggest that the HCl-initiated ring-opening of $[PCl_2N]_3$ follows a two-step process (Scheme 4). Before the reaction begins, HCl is hydrogen-bonded to a nitrogen atom in $[PCl_2N]_3$, and this N–H bond distance is 1.888 Å at the MP2/aTZ level of theory. The reactant (**R′**) reaches the first transition state (**TS1′**) (by overcoming an energy barrier of 116.48 kJ mol^{-1}, Table 3), in which the H–Cl bond is lengthened to 1.957 Å. The stretched HCl bond also delivers the Cl atom to a unique bridging position that is only 2.683 Å away

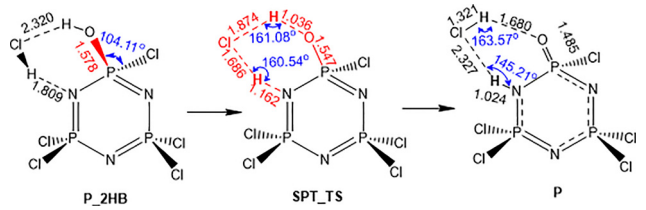

Scheme 3 The reactants, transition state and the product of the HCl-catalyzed tautomerization of the hydrolyzed product calculated at the MP2/aTZ level of theory. This reaction is a continuation of hydrolysis shown in Scheme 1.

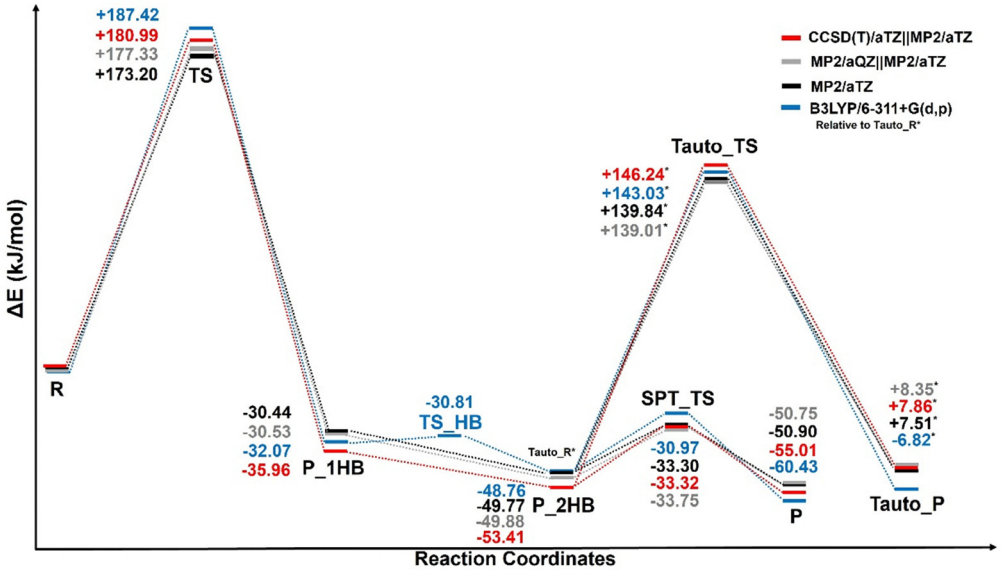

Fig. 1 The potential energy surface diagram of the hydrolysis followed by the HCl-catalyzed tautomerization probed at four different levels of theory: MP2/aXZ where X = T and Q, CCSD(T)/aTZ based on the MP2/aTZ optimized structures, as well as B3LYP/6-311+G(d,p). Two different pathways were depicted starting at **P_2HB**, where energy values denoted with * are from the pathway without HCl.

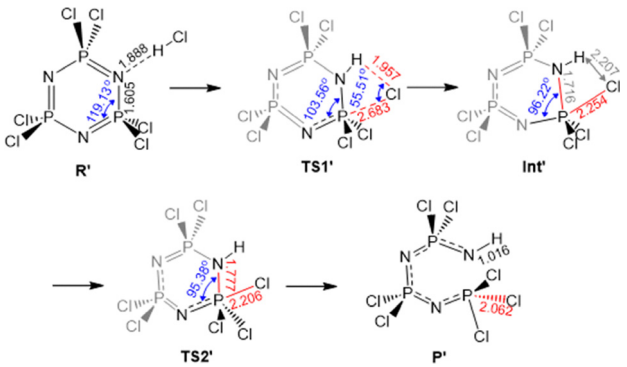

Scheme 4 The five stationary points for the two-step, HCl-initiated $[PCl_2N]_3$ ring-opening reaction, characterized at the MP2/aTZ level of theory.

from the neighboring P atom, deforming the tetrahedral P atom into a distorted bipyramid structure. Compared to the reactant (**R**′), the N–P–N bond angle decreases from 119.13° to 103.56°. The cleavage of the H–Cl bond and the formation of the P–Cl bond relax **TS1**′ into intermediate **Int**′ and releases *ca.* 14.38 kJ mol^{-1} of heat. The Cl atom of the P–Cl bond in **Int**′ is 2.254 Å from P and 2.207 Å from H, while the N–P–N bond angle further decreases to 96.22° indicating a trigonal bipyramidal structure of the P center. The protonation of N and the geometry change occurring at the P center noticeably increase the P–N bond length from 1.605 Å to 1.716 Å. **Int**′ requires less than 14.00 kJ mol^{-1} to reach the second transition state (**TS2**′), making **Int**′ relatively unstable (low-lying **TS2**′). As the P–Cl bond is shortened to 2.206 Å, the P–N bond further elongates to 1.777 Å, and at the same time, the N–P–N bond angle slightly decreases to 95.38°. Finally, the bipyramidal P reverts back to a tetrahedral structure along with the cleavage of the P–N bond and an energy release of 31.53 kJ mol^{-1}. The Cl from the HCl remains bound to P with a P–Cl bond length of 2.062 Å.

Further MP2/aQZ and CCSD(T)/aTZ single-point energy calculations on MP2/aTZ geometry optimized structures are consistent with the MP2/aTZ results (Table 3 and Table S6), as the energy differences for each step differ by no more than 4 kJ mol^{-1} and 6 kJ mol^{-1}, respectively. Although all 7 DFT functionals tested can provide a good description of the stepwise reaction mechanism, the energies obtained at the B3LYP/6-311+G(d,p) level of theory present a remarkable accuracy when compared to ΔE obtained at the MP2/aQZ||MP2/aTZ level of theory. With the deviations no more than *ca.* 4% throughout the whole mechanistic pathway (Table S6), B3LYP/6-311+G(d,p) stands out as a fast yet promising combination to reproduce near "gold-standard" *ab initio* energetics for the small/medium-sized phosphazene systems that contain N, P, Cl and H atoms only.

This aligns with the previous observations reported in the hydrolysis and tautomerization of chlorophosphazenes.[57]

To shed light on how the existence of HCl can interfere $[PCl_2N]_3$ from interacting with each other and proceed with polymerization, the rate constants of the rate-determining steps in the two reactions were extrapolated and compared. For example, at 500 K, HCl can ring-open $[PCl_2N]_3$ faster than a neighboring $[PCl_2N]_3$ on a 10^{12} scale, suggesting that HCl can initiate and proceed with ring-opening of $[PCl_2N]_3$ much faster than another $[PCl_2N]_3$, which can substantially interfere with the targeted polymerization reactions.

3.2 Frontier molecular orbitals (FMO), electrostatic potential (ESP), and natural bond orbital (NBO) analysis

3.2.1 Hydrolysis of $[PCl_2N]_3$. The electronic features associated with the hydrolysis of $[PCl_2N]_3$ (Scheme 1) were

Table 3 The relative energies (ΔE, in kJ mol^{-1}) of the stationary points from the ring-opening reaction initiated by HCl determined at different DFT levels of theory, the MP2/aXZ levels of theory where X = D, T and Q and the CCSD(T)/aTZ level of theory

	DFT								*Ab initio*			
Theory F/M[a]	B3LYP		B3LYP-D3	B3PW91	ωB97X-D	M06-2X	cam-B3LYP	PBE0	MP2			CCSD(T)
Cmpd/B[b]	aTZ	6-311+G(d,p)							aDZ	aTZ	aQZ[c]	aTZ[c]
R′	0.00	0.00	0.00	0.00	0.00	0.00	0.00	0.00	0.00	0.00	0.00	0.00
TS1′	116.13	115.84	109.04	113.13	124.00	113.06	121.45	111.75	111.00	116.48	117.33	118.82
Int′	114.43	113.31	104.75	107.76	117.45	101.55	117.67	104.68	94.45	102.10	104.09	108.95
TS2′	124.84	120.84	113.26	115.01	126.00	110.49	126.67	112.55	107.54	115.52	118.58	121.19
P′	96.23	92.88	83.84	86.82	94.59	76.95	95.80	83.38	74.41	83.99	86.74	89.76

[a] Functional or method. [b] Compound and basis set. [c] Single-point energies completed based on the electronic structures fully optimized at the MP2/aTZ level of theory.

examined through a frontier molecular orbital (FMO) analysis of the MP2/aTZ geometry-optimized stationary points. Changes in orbital energies and spatial distributions along the reaction coordinate provide insight into the electronic factors governing nucleophilic attack, P–Cl bond cleavage, and subsequent hydrogen-bond stabilization.

From the reactant to the transition state, a decrease in the HOMO–LUMO energy gap (ΔE) is observed, consistent with increased orbital interaction and enhanced reactivity at the phosphorus center. In the reactant, the HOMO and HOMO−1 are predominantly localized on the chlorophosphazene ring, whereas the LUMO exhibits significant amplitude at the P–Cl bonds and the approaching oxygen atom of water. At the transition state, the LUMO becomes increasingly localized in the –N–P–Cl···O region, reflecting charge acceptance during nucleophilic attack and the concurrent weakening of the P–Cl bond. The energy differences between the HOMO and HOMO−1 orbitals, centered on the ring system (with the exception of **SPT_TS** in the tautomerization process) are 0.0460, 0.362, 0.0702, 0.0716, 0.165, and 0.498 eV for **R**, **TS**, **P_1HB**, **P_2HB**, **SPT_TS**, and **P** respectively (Fig. 2). This change in the orbital configuration along the **R**/**TS**/**P_1HB** pathway, which is characterized by a significant increase in separation between HOMO and HOMO−1 energy levels, shows that the simple change of having the small HCl molecule present induces a substantial electronic reorganization. This perturbation is not limited to the Frontier orbitals but propagates throughout the lower lying valence levels. This highlights the pronounced electronic effects that the presence of HCl has on these systems. This is especially noteworthy in chlorophosphazene synthesis since HCl production is ubiquitous in a chlorophosphazene reaction. The spread of the electron density in the canonical orbitals of the reactants and products shows the stabilizing effect that this electron distribution brings to these structures as well as the presence of a more localized orbital configuration at the transition state with a smaller HOMO–LUMO gap and a simultaneous increase in the HOMO–HOMO−1 gap, which indicates the prevalence of reactivity residing in the higher energy occupied orbitals in this reaction. Therefore, the presence or the absence of HCl during this reaction can play an important role in the synthesis of chlorophosphazenes. The difference in E_a for HCl catalyzed tautomerization (Fig. 1) highlights the significance of hydrogen bonding and urges us to revisit how it can facilitate a proton transfer. This discovery prompted us to further explore an anticipated focal point for our analysis and

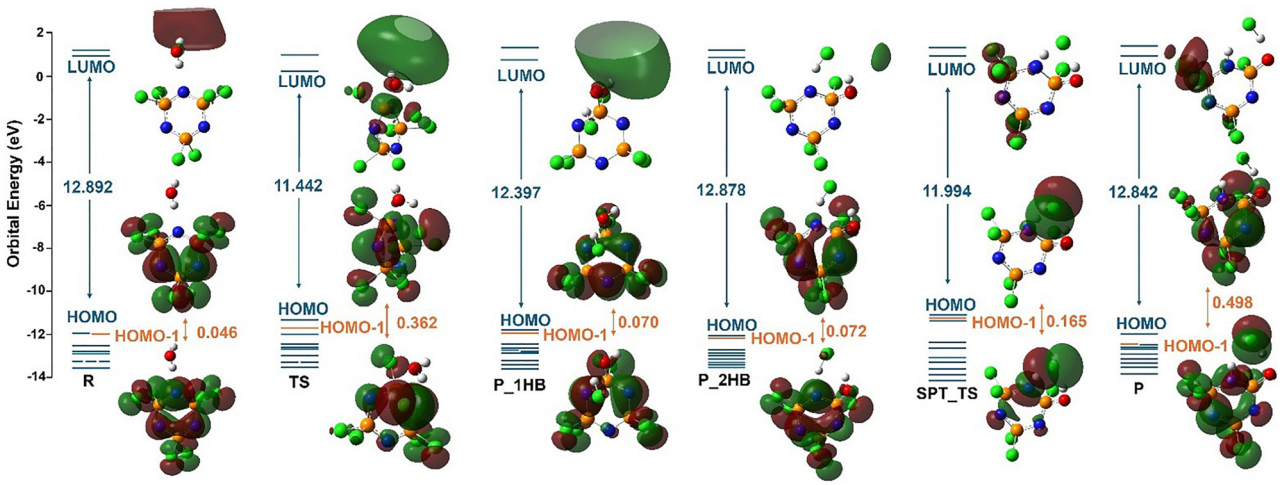

Fig. 2 The energy gaps between the HOMO/LUMO (marked in blue) and HOMO/HOMO−1 for the HCl catalyzed hydrolysis reaction (Fig. 1) estimated from SCF FMOs calculated at the MP2/aTZ level of theory.

a possible tautomerization process. As summarized in Fig. 2, the FMOs of the two products with differing hydrogen-bonding arrangements provide clear evidence for an HCl-catalyzed tautomerization process, underscoring the critical role of hydrogen bonding in lowering the barrier to proton transfer.

A comparative analysis of the FMOs for catalyzed and uncatalyzed tautomerization (Fig. 1) indicates that, in the absence of catalytic lowering of the activation energy (E_a), the HOMO–LUMO energy gaps (ΔE) are 12.409 eV for **Tauto_R**, 12.844 eV for **Tauto_TS**, and 12.484 eV for **Tauto_P**. These values show that the transition state of the uncatalyzed tautomerization possesses a larger HOMO–LUMO gap than those of both the reactants and products. In contrast, for the catalyzed tautomerization (Fig. 3), the HOMO–LUMO ΔE values are 12.878 eV for **P_2HB**, 11.994 eV for **SPT_TS**, and 12.842 eV for **P**, demonstrating a reduced HOMO–LUMO gap for the catalyzed transition state. This reduction suggests that, provided the activation energy barrier can be overcome (Fig. 1), formation of the HCl-catalyzed tautomer is highly probable in chlorophosphazene reactions.

Examination of the HOMO/HOMO−1 energy gap (E_{gap}) further supports this conclusion. As shown in Fig. 2, HCl-catalyzed tautomerization leads to an order-of-magnitude increase in E_{gap} from the reactant to product **P**; notably, the gap approximately triples through tautomerization alone (Fig. 3), indicating stabilization *via* lowering of inner orbital energies. In contrast, the uncatalyzed process exhibits the opposite behavior, with the HOMO/HOMO−1 E_{gap} decreasing by approximately a factor of five (Fig. 3). This progressive orbital stabilization provides a direct electronic link between hydrolysis and the subsequent HCl-catalyzed tautomerization discussed previously. In particular, the hydrogen-bond-mediated lowering of frontier orbital energies in **P_2HB** facilitates proton transfer by stabilizing the synchronous proton-transfer transition state (Fig. 2 and 3). Therefore, this process has a pronounced influence on both system stability and reactivity, underscoring the critical role of HCl in processes such as chlorophosphazene ring hydrolysis and in facilitating tautomerization during these reactions.

Building on the stabilizing influence of hydrogen bonding discussed above, the role of HCl in this system was examined in greater detail through further analysis of **P_2HB**. This investigation revealed that orbital mixing between the formed HCl and the chlorophosphazene ring is not observed within the next ten lowest occupied molecular orbitals. However, closer examination uncovered a subsequent low-activation energy step (Scheme 3) that leads to the formation of a second hydrogen bond in the reaction site (–P–O–H···Cl–H···N–). Fig. 4 illustrates the HOMO and HOMO−6 orbitals associated with this hydrogen-bonding region, as calculated at both the MP2/aTZ and B3LYP/6-311+G(d,p) levels of theory. The close agreement between these results at different levels of theory demonstrates that both methods provide highly comparable orbital descriptions, with the DFT approach offering a significantly more cost-effective computational alternative.

Along with the FMO analysis, NBO calculations and electrostatic potential (ESP) mapping at the MP2/aTZ level of theory also show a clear progression of electron density through the hydrolysis reaction. The electron density redistributes through the core of the reaction site, while the phosphorus atom experiences only minimal variation in its positive charge (Fig. 5: +2.046 for **R**, 2.048 for **TS**, and 2.046 for **P_2HB**). This indicates that the phosphorus center plays a relatively minor role in the electron density shifts compared to the nitrogen and chlorine atoms. In contrast, the transferring chlorine atom shows a substantial increase in its negative charge, changing from −0.237 (**R**) to −0.549 (**TS**), and then to −0.330 (**P_2HB**). As the reaction proceeds, this chlorine atom donates electron density to form a covalent H–Cl bond with one of the hydrogen atoms of the water molecule, yielding an HCl bond length of 1.31 Å (Fig. 5).

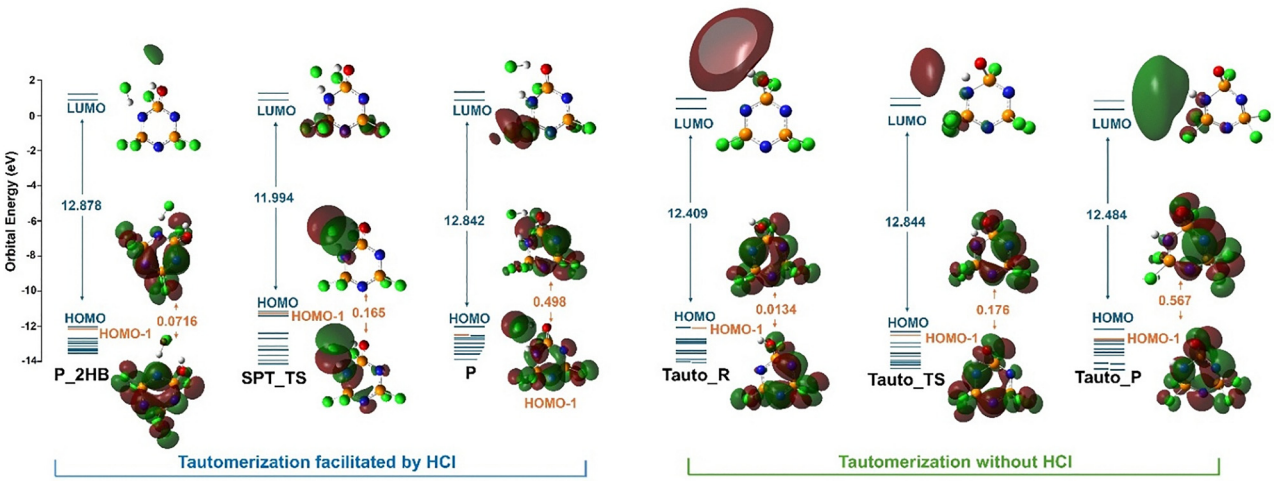

Fig. 3 The HCl catalyzed and noncatalyzed tautomerization comparison of the HOMO/LUMO energy gap and the energy difference of the HOMO/HOMO−1 (Fig. 1) estimated from SCF FMOs calculated at the MP2/aTZ level of theory.

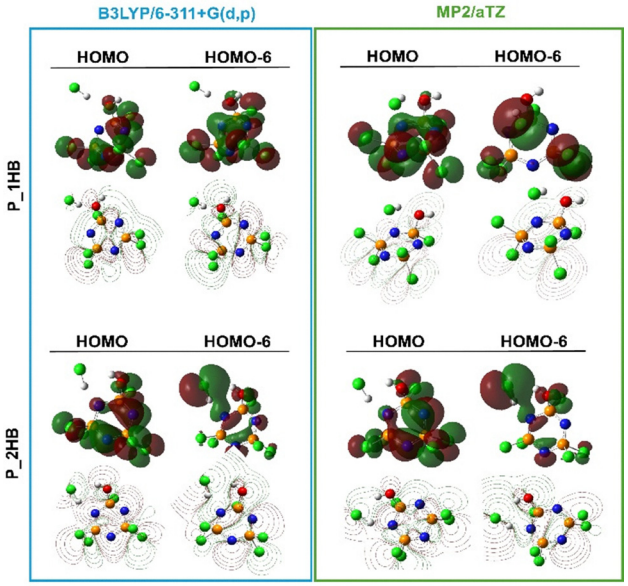

Fig. 4 The HOMO and HOMO−6 orbitals of the products **P_1HB** and **P_2HB** with two different hydrogen bond configurations fully optimized at the B3LYP/6-311+G(d,p) and MP2/aTZ levels of theory.

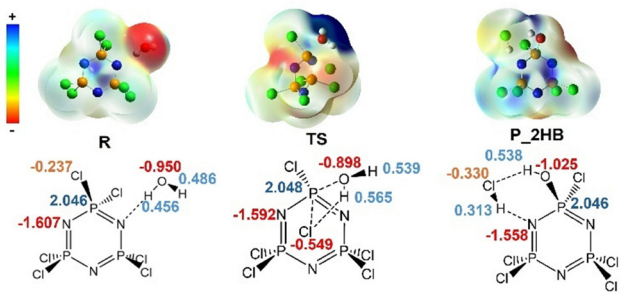

Fig. 5 ESP maps (-3.000×10^{-2} to 3.000×10^{2}) along with the corresponding atomic point charges (a.u.) in the core reactive site for the hydrolysis reaction (Scheme 1) calculated at the MP2/aTZ level.

Overall, the FMO analysis suggests that hydrogen bonding to the HCl byproduct plays a decisive role in stabilizing hydrolysis products and shaping the electronic landscape for downstream reactivity. The strong proton acceptor character of Cl^{-} that develops in the TS, as well as the formation of hydrogen bonds produces a better alignment of the proton with the H-donor (N) and H-acceptor (Cl^{-}), thus providing an enhanced interaction compared to the constrained N–H···O geometry, leading to a strong cooperative intermolecular hydrogen bond network and thereby substantially lowering the energy barrier.

3.2.2 Two-step $[PCl_2N]_3$ ring-opening reaction initiated by HCl. As can be seen in the hydrolysis and in the HCl ring-opening reactions of chlorophosphazenes, the degenerate HOMO and HOMO−1 (Table S21) orbitals, explored previously in the literature for the $[PCl_2N]_3$ ring,[67] show similar configurations in this study for the reactants (Fig. 6). The inner bonding orbital HOMO−2 (Table S21 and Fig. S1) shows an

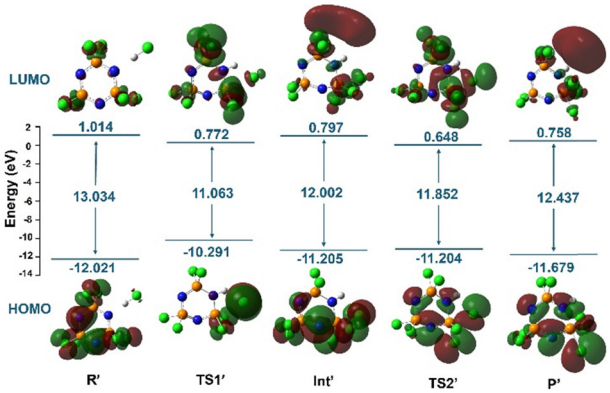

Fig. 6 The HOMO–LUMO orbitals and energy gap (ΔE) comparison for the two-step $[PCl_2N]_3$ ring-opening reaction initiated by HCl (estimated from SCF FMOs calculated at the MP2/aTZ level).

orbital extending to cover the reactive site in **TS1′** stabilizing the proton transfer and charge redistribution to the migrating chloride atom. The **TS2′** further shows extended electron delocalization and stabilization at the nitrogen and phosphorus reactive sites with a slight shortening of the N–P bond of the anterior side of the reactive phosphorus center (Table S19), which allows for the lengthening and ultimately breaking the P–N bond and the formation of the ring opened product. The intermediate and product have extensively delocalized LUMO orbitals which may indicate a highly reactive site where electron rich reagents could further interact with the new

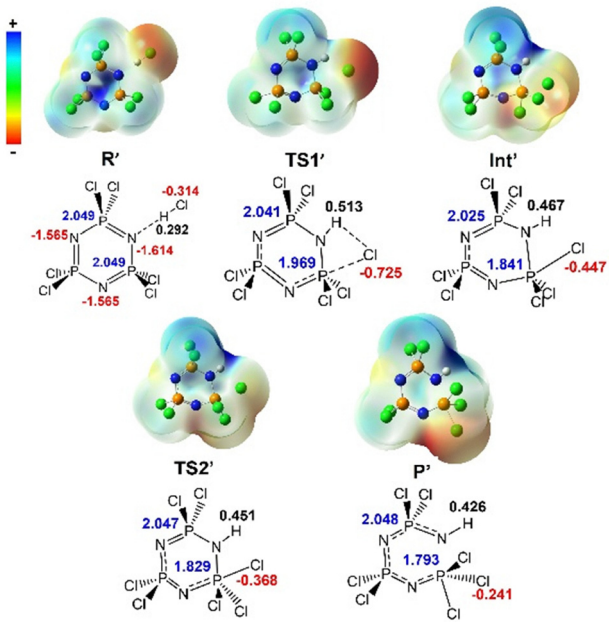

Fig. 7 ESP maps (-3.506×10^{-2} to 3.506×10^{2}), annotated with atom labels and accompanied by a charge trend table, highlighting the reactive behavior of the phosphorus center and the formation of the ring-opened product following the hydrogen transfer to nitrogen for the HCl-initiated $[PCl_2N]_3$ ring-opening reaction calculated at the MP2/aTZ level (Scheme 4).

phosphorus tail that could be the focus of an electrophilic attack.

Unlike what was observed in the hydrolysis reaction, where the charge of the phosphorus center changes only very little, the two-step $[PCl_2N]_3$ ring-opening reaction initiated by HCl shows a large change in charge at the phosphorus center (Fig. 7). The transferred chlorine also shows large changes in its point charge, most notably through the first transition state where its charge more than doubles as the hydrogen is fully transferred to the ring nitrogen. In this process the interaction between the nitrogen and hydrogen shows a donation of charge density from the nitrogen to the hydrogen to form the molecular bond and subsequently shows very little change in their charges for the remainder of the reaction. The charge density of the reactive chlorine being relocated is gradually transferred to the reactive phosphorus center disrupting the N–P bond by lengthening and ultimately breaking it to produce the ring-opened product (Fig. 7 and Tables S16–S20).

4. Conclusions

Through both MP2 and CCSD(T) *ab initio* methods as well as various DFT functionals, this work thoroughly investigates the mechanism of the $[PCl_2N]_3$ reaction with small molecules like H_2O and HCl in a 1 : 1 ratio. Our QM calculations indicate that $[PCl_2N]_3$ hydrolysis is triggered by a strong non-covalent interaction between the N in the $[PCl_2N]_3$ and the H in H_2O and could be completed in one step. The reaction with HCl requires a lower activation energy (*ca.* 180 kJ mol^{-1} calculated at the CCSD(T)/aTZ‖MP2/aTZ level of theory) than the ring-opening polymerization and ring–ring expansion equilibrium, which requires *ca.* 240 kJ mol^{-1} of energy (determined at a comparable B3LYP/6-311+G(d) DFT level of theory).[89]

Built on previous experimental work on the tautomerization pathway of $P_3N_3Cl_5OH$,[57] this study also investigated the one-step mechanism of this reaction. When the reaction occurs without interference from any other proton source, the proton transfer between the –OH and N in $P_3N_3Cl_5OH$ follows a single-step mechanism and completes after overcoming an E_a of *ca.* 139 kJ mol^{-1} calculated at the MP2/aTZ level of theory. Interestingly, $P_3N_3Cl_5OH$ can trap HCl *via* two hydrogen bonds, and the special configuration triggers the HCl-catalyzed tautomerization *via* a synchronous proton transfer. This process has a significantly lower activation energy (16.47 kJ mol^{-1}), demonstrating a 90% reduction in the demanded energy input when compared with the uncatalyzed tautomerization. Moreover, the ability of this reaction to generate HCl as a byproduct, which actively participates in the following tautomerization and ring-opening reactions, makes it a pivotal step in preventing side reactions in ring-opening polymerizations. On the other hand, once HCl is generated, it will cleave the cyclic $[PCl_2N]_3$ in two steps, and as a result, a linear product with a –NH terminus is formed. Interestingly, the HCl-initiated ring-opening requires much less energy input than the ring–ring equilibrium, as well as the ring-initiated polymerization for tadpole formation.[89] This sheds light on the role of HCl as a Lewis acid in polymerization reactions and why it can disrupt the complex polymerization process. Further kinetics studies on the reaction rate constants for pivotal rate-determining steps revealed the significant differences triggered by HCl and H_2O and support the mechanistic point presented here, *i.e.* small molecule acid/base chemistry (H_2O/HCl) can open lower-barrier pathways that compete with or even disrupt polymerization chemistry. We see this very clearly in our results once HCl is present in the reaction.

This, to the best of our knowledge, is the first systematic theoretical study of the interactions between a single $[PCl_2N]_3$ ring and small molecules like H_2O and HCl as two different proton sources. Along with the novel mechanistic findings, our efforts in both the DFT and *ab initio* MP2 and CCSD(T) calculations indicate that when comparing the E_a and ΔH probed at the MP2/aQZ‖MP2/aTZ and DFT levels of theory the DFT energetics are always within *ca.* 6% and 3% deviation, respectively, suggesting that the DFT combination of the B3LYP functional with the 6-311+G(d,p) basis set is an excellent computational tool to study the reactivity of phosphazene systems and their reactions, with the additional benefits of being much faster and more computationally affordable, yet still providing a reliable QM approach to reproduce the *ab initio* MP2 and CCSD(T) results obtained with large basis sets.[68,89,90]

Conflicts of interest

There are no conflicts to declare.

Abbreviations

PES	Potential energy surface
MP2	*Ab initio* second-order Møller–Plesset perturbation theory
SCF	Self-consistent field
HOMO and LUMO	Highest occupied molecular orbital and lowest unoccupied molecular orbital, respectively
ESP map	Electrostatic potential map
NBO	Natural bond orbital
DFT	Density functional theory
n_i	The number of imaginary frequencies
CCSD(T)	The coupled cluster singles, doubles, and perturbative triples

Data availability

The data supporting this article have been included as part of the supplementary information (SI). Supplementary information: Section S1. Selected paths and activation energies for critical steps in the reaction of chlorophosphazene with H_2O and HCl determined at different levels of QM theories and their accuracy when compared to the results at the CCSD(T)/aTZ||MP2/aTZ level of theory. Section S2. Harmonic vibrational

frequencies (ω in cm^{-1}) and infrared intensities (IR in km mol^{-1}) for the pivotal minima in the reaction mechanisms. Section S3. Bond lengths for chemical species appearing in the ring-opening reaction at the MP2/aTZ level of theory. Section S4. The energies and shapes of the frontier molecular orbitals of selected structures. Section S5. Cartesian coordinates for all stationary points optimized at different levels of theory. See DOI: https://doi.org/10.1039/d5cp05068e.

Acknowledgements

This work was supported by the computational grants PWOO0015 and POBC0041 from the Ohio Supercomputer Center and the Advanced Cyberinfrastructure Coordination Ecosystem: Services & Support (ACCESS) program (supported by the National Science Foundation grants #2138259, #2138286, #2138307, #2137603, and #2138296) through allocation MCB170023. Y. X. and C. R. S. acknowledge technical help and support from the Ohio Supercomputer Center. Y. X. also acknowledges the Mississippi Center for Supercomputing Research for access to their computational resources and the support from the University of Mississippi. This work was also partially supported by grants from the National Institutes of Health P01HL147823, R01HL103866 and R01NS124547.

References

1 V. Petro and S. Shore, *J. Am. Chem. Soc.*, 1964, 336–338.
2 I. S. Sirotin, Y. V. Bilichenko, O. V. Suraeva, A. N. Solodukhin and V. V. Kireev, *Polym. Sci., Ser. B*, 2013, **55**, 63–68.
3 G. Nichols, *Process for Preparing Phosphonitrilic Chloride Polymers*, US3249397, 1966.
4 N. Paddock, *Production of phosphonitrilic oils*, US3026174, 1962.
5 H. Allcock, S. Stinnett, J. Tedder and J. Adams, US4656017, 1987.
6 J. Teja and R. Peters, US2788286, 1957.
7 P. L. Silvestrelli, M. Gleria, R. Milani and A. B. Boscoletto, *J. Inorg. Organomet. Polym. Mater.*, 2006, **16**, 327–341.
8 J. Emsley and P. Udy, *J. Chem. Soc. A*, 1971, 768–772.
9 J. Emsley and P. Udy, *J. Chem. Soc. A*, 1970, 3025–3029.
10 H. Allcock, *Chemistry and Applications of Polyphosphazenes*, Wiley – Interscience, Hoboken, New Jersey, 2003, vol. 41.
11 L. Lund, N. Paddock, J. Proctor and H. Searle, *J. Chem. Soc.*, 1960, 2542–2548.
12 J. Emsley and P. Udy, *Chem. Commun.*, 1967, 633–634.
13 V. Binder and E. Fluck, *Z. Anorg. Allg. Chem.*, 1971, **381**, 21–30.
14 C. Zhang and Y. Yong, *Henan Shifan Daxue Xuebao, Ziran Kexueban*, 2008, **36**(4), 168–170.
15 P. Potin and R. D. Jaeger, *Eur. Polym. J.*, 1991, **27**, 341–348.
16 H. Allcock, *Chemistry and Applications of Polyphosphazenes*, Wiley – Interscience, Hoboken, New Jersey, 2003, pp. 137–187.
17 I. Alkorta and J. Elguero, *Phosphorus, Sulfur Silicon Relat. Elem.*, 2019, **195**, 307–313.
18 H. Allcock, *Chem. Rev.*, 1972, **72**, 315–356.
19 H. Allcock, *Dalton Trans.*, 2016, **45**, 1856–1862.
20 L. F. Audrieth, R. Steinman and A. D. F. Toy, *Chem. Rev.*, 1943, **32**, 109–133.
21 R. Shaw, B. Fitsimmons and B. Smith, *Chem. Rev.*, 1962, **62**, 247–281.
22 H. R. Allcock, *Curr. Opin. Solid State Mater. Sci.*, 2006, **10**, 231–240.
23 S. Rothemund and I. Teasdale, *Chem. Soc. Rev.*, 2016, **45**, 5200–5215.
24 N. Paddock, Phosphonitrilic Derivatives and Related Compounds, *Q. Rev., Chem. Soc.*, 1964, 168–210.
25 M. Gleria and R. De Jaeger, *Top. Curr. Chem.*, 2005, **250**, 165–251.
26 H. Allcock, *Chemistry and Applications of Polyphosphazenes*, Wiley – Interscience, Hoboken, New Jersey, 2003, vol. 3–26, pp. 109–136.
27 F. F. Stewart, *Organophosphorous Chemistry – Phosphazenes*, 2012, pp. 249–384.
28 V. Chandrasekhar and R. S. Narayanan, in *Organophosphorus Chemistry*, ed. D. W. Allen, D. Loakes and J. C. Tebby, The Royal Society of Chemistry, 2017, vol. 46, pp. 342–417.
29 V. Chandrasekhar and R. S. Narayanan, in *Organophosphorus Chemistry*, ed. D. W. Allen, D. Loakes and J. C. Tebby, The Royal Society of Chemistry, 2016, vol. 45, pp. 375–437.
30 K. Wang, J. G. Zhang, H. H. Zheng, H. S. Huang and T. L. Zhang, *Quantum Chemistry – Molecules for Innovation*, 2012, vol. 175.
31 R. Pajkert and G.-V. Röschenthaler, *Organophosphorus Chemistry*, The Royal Society of Chemistry, Cambridge, 2016, vol. 45, pp. 354–374.
32 Y. Kondo, *Superbases for Organic Synthesis: Guanidines, Amidines, Phosphazenes and Related Organocatalysts*, Wiley Online Library, 2009, pp. 145–185.
33 H. Allcock, *ACS Symposium Series*, 2018, ch. 21, vol. 1298, pp. 3–26.
34 H. Allcock and N. Morozowich, *Polym. Chem.*, 2012, **3**, 578–590.
35 A. K. Andrianov, *J. Inorg. Organomet. Polym. Mater.*, 2006, **16**, 397–406.
36 A. K. Andrianov, D. P. DeCollibus, H. A. Gillis, H. H. Kha, A. Marin, M. R. Prausnitz, L. A. Babiuk, H. Townsend and G. Mutwiri, *Proc. Natl. Acad. Sci. U. S. A.*, 2009, **106**, 18936–18941.
37 A. K. Andrianov, J. R. Sargent, S. S. Sule, M. P. Le Golvan, A. L. Woods, S. A. Jenkins and L. G. Payne, *J. Bioact. Compat. Polym.*, 2016, **13**, 243–256.
38 L. Ai, S. Chen, J. Zeng, P. Liu, W. Liu, Y. Pan and D. Liu, *Polym. Degrad. Stab.*, 2018, **155**, 250–261.
39 Y. C. Stone D. and H. Allcock, *J. Polym. Sci., Part A: Polym. Chem.*, 2006, **44**, 69–76.
40 R. Sharma, R. K. Rawal, M. Malhotra, A. K. Sharma and T. R. Bhardwaj, *Bioorg. Med. Chem.*, 2014, **22**, 1104–1114.

41 H. R. Allcock, L. B. Steely and A. Singh, *Polym. Int.*, 2006, **55**, 621–625.
42 C. W. Allen, *J. Inorg. Organomet. Polym. Mater.*, 2006, **16**, 273–276.
43 H. Honarkar and A. Rahimi, *Monatsh. Chem.*, 2007, **138**, 923–933.
44 N. Yevlampieva, D. Tur, A. Kovshik and E. Rjumtsev, *J. Inorg. Organomet. Polym. Mater.*, 2012, **22**, 1156–1164.
45 J. Luten, J. H. van Steenis, R. van Someren, J. Kemmink, N. M. E. Schuurmans-Nieuwenbroek, G. A. Koning, D. J. A. Crommelin, C. F. van Nostrum and W. E. Hennink, *J. Controlled Release*, 2003, **89**, 483–497.
46 C. Zheng, L. Qiu and K. Zhu, *Polymer*, 2009, **50**, 1173–1177.
47 S. Wilfert, A. Iturmendi, W. Schoefberger, K. Kryeziu, P. Heffeter, W. Berger, O. Bruggemann and I. Teasdale, *J. Polym. Sci., Part A: Polym. Chem.*, 2014, **52**, 287–294.
48 R. Wycisk and P. N. Pintauro, *Fuel Cells II*, 2008, pp. 157–183.
49 T. Fushimi and H. R. Allcock, *Dalton Trans.*, 2009, 2477–2481.
50 C. G. Valenzuela C., M. Valenzuela, L. Zuniga and C. O'Dwyer, *J. Inorg. Organomet. Polym. Mater.*, 2012, **22**, 447–454.
51 I. Teasdale and O. Bruggemann, *Polymers*, 2013, **5**, 161–187.
52 N. S. Başterzi, S. Bilge Koçak, A. Okumuş, Z. Kılıç, T. Hökelek, Ö. Çelik, M. Türk, L. Y. Koç, L. Açık and B. Aydın, *New J. Chem.*, 2015, **39**, 8825–8839.
53 A. Uslu, S. O. Tümay and S. Yeşilot, *J. Photochem. Photobiol., C*, 2022, 100553.
54 R. E. Singler, M. S. Sennett and R. A. Willingham, *Inorganic and Organometallic Polymers: ACS Spymposium Series, CH20*, 1988, vol. 360, pp. 268–276.
55 M. Gleria and R. D. Jaeger, Polyphosphazenes: A Review, *Top. Curr. Chem.*, 2005, **250**, 165–251.
56 J. Emsley and P. Udy, *Polymer*, 1972, **13**, 593–594.
57 (*a*) D. G. Gabler and J. F. Haw, *Inorg. Chem.*, 1990, **29**, 4018–4021; (*b*) B. De Ruiter, H. Winter, T. Wilting and J. C. van de Grampel, *J. Chem. Soc., Dalton Trans.*, 1984, **6**, 1027; (*c*) R. Hayes and C. Allen, *Dalton Trans.*, 2016, **45**, 2060–2068.
58 L. M. Frutos, G. A. Carriedo, M. P. Tarazona and E. Saiz, *Macromolecules*, 2009, **42**, 8769–8773.
59 H. Allcock and R. Kugel, *J. Am. Chem. Soc.*, 1965, **87**, 4216–4217.
60 N. G. Pollard F. and R. Warrender, *J. Chromatogr.*, 1962, **9**, 483–492.
61 H. Allcock, J. Gardner and K. Smeltz, *Use of Water as a Catalyst for the Polymerization of Chlorophosphazenes*, US3937790, 1976.
62 J. L. Kroger, J. R. Fried and A. A. Skelton, *Int. J. Quantum Chem.*, 2013, **113**, 63–70.
63 M. Gorlov, N. Bredov, A. Esin, I. Sirotin, M. Soldatov, V. Oberemok and V. V. Kireev, *Int. J. Mol. Sci.*, 2021, **22**, 5958.
64 M. Becke-Goehring and E. Fluck, *Angew. Chem.*, 1962, **1**, 281–285.
65 H. Allcock, J. Gardner and K. Smeltz, *Macromolecules*, 1975, **8**, 36.
66 W. Haubold and E. Fluck, *Kernmagnetihe Resonnz Von Phosphorverbinungen*, 1971, vol. 28, pp. 368–376.
67 R. Jaeger, M. Debowski, I. Manners and G. J. Vancso, *Inorg. Chem.*, 1999, **38**, 1153–1159.
68 C. Salmon, Y. Xue and V. Gogonea, *Inorg. Chem.*, 2023, **62**, 19412–19420.
69 W. M. Zoghaib, J. Husband, U. A. Soliman, I. A. Shaaban and T. A. Mohamed, *Spectrochim. Acta, Part A*, 2013, **105**, 446–455.
70 V. Jancik, F. Cortes-Guzman, R. Herbst-Irmer and D. Matinez-Otero, *Chem. – Eur. J.*, 2017, **23**, 6964–6968.
71 A. Chaplin, J. Harrison and P. Dyson, *Inorg. Chem.*, 2005, **44**, 8407–8417.
72 M. Breza and S. Biskupic, *J. Mol. Struct.: THEOCHEM*, 1995, **332**, 277–281.
73 M. Breza, *J. Mol. Struct.: THEOCHEM*, 1998, **454**, 77–81.
74 M. Breza, *Polyhedron*, 2000, **19**, 389–397.
75 M. Breza, *J. Mol. Struct.: THEOCHEM*, 2000, **505**, 169–177.
76 M. Breza, *Polyhedron*, 2003, **22**, 3243–3248.
77 M. Enlow, *Polyhedron*, 2003, **22**, 473–482.
78 M. Breza, *J. Mol. Struct.: THEOCHEM*, 2004, **679**, 131–136.
79 M. F. Bobrov, G. V. Popova and V. G. Tsirelson, *Russ. J. Phys. Chem.*, 2006, **80**, 584–590.
80 L. Kapička, P. Kubáček and P. Holub, *J. Mol. Struct.: THEOCHEM*, 2007, **820**, 148–158.
81 M. S. Sadjadi, B. Sadeghi and K. Zare, *J. Mol. Struct.: THEOCHEM*, 2007, **817**, 27–33.
82 M. Gall and M. Breza, *J. Mol. Struct.: THEOCHEM*, 2008, **861**, 33–38.
83 T. Kupka, K. Pasterny, G. Pasterna and K. Brandt, *J. Mol. Struct.: THEOCHEM*, 2008, **866**, 21–26.
84 M. L. Abdellatif, B. Maouche, Y. Belmiloud, N. Triaki and M. Brahimi, *Open Struct. Biol. J.*, 2009, **3**, 26–33.
85 I. I. Vorontsov, D. R. Tur, V. S. Papkov and M. Y. Antipin, *J. Mol. Struct.*, 2009, **928**, 1–11.
86 R. J. Davidson, E. W. Ainscough, A. M. Brodie, J. A. Harrison and M. R. Waterland, *Eur. J. Inorg. Chem.*, 2010, 1619–1625.
87 I. Alkorta, J. Elguero and A. Fruchier, *Magn. Reson. Chem.*, 2019, **57**, 975–981.
88 A. Schulz, M. Thormählen and H. C. Müller, *Internet Electron. J. Mol. Des.*, 2003, **2**, 653–677.
89 Y. Xue, C. R. Salmon, S. E. Ramlo, W.-Y. Chen, V. Gogonea and C. A. Tessier, *Macromolecules*, 2024, **5**, 1.
90 C. Salmon, Y. Xue, E. Yeo, V. Gogonea and S. Ramlo, *J. Heterocycl. Chem.*, 2025, **62**, 12.
91 A. Y. Tolbin, B. N. Tarasevich, M. K. Beklemishev, V. K. Brel and V. E. Pushkarev, *ChemistrySelect*, 2022, **7**, e202201065.
92 M. L. Valenzuela, D. MacLeod-Carey, C. S. Marfull, J. Leon-Baeza, J. Martínez, A. Antinolo and F. Carrillo, *J. Inorg. Organomet. Polym. Mater.*, 2022, **32**, 1724–1735.
93 A. R. Keating-Zaid, Doctoral dissertation, The University of Akron, 2023.

94 M. Gall and M. Breza, *Int. J. Quantum Chem.*, 2021, **121**, e26613.
95 R. Ramirez-Tagle and L. Alvarez-Thon, *Int. J. Quantum Chem.*, 2024, **124**, e27431.
96 S. Muhammed, H. Manojkumar and P. Parameswaran, *ChemistrySelect*, 2024, **9**, e202304332.
97 O. Dagdag and H. Kim, *Polymers*, 2023, **16**, 122.
98 S. O. Tümay, A. Şenocak, B. Çoşut, H. A. Alidağı and S. Yeş ilot, *Photochem. Photobiol. Sci.*, 2023, **22**, 1429–1444.
99 A. Otero-De-La-Roza, E. R. Johnson and J. Contreras-García, *Phys. Chem. Chem. Phys.*, 2012, **14**, 12165–12172.
100 M. J. Frisch, G. W. Trucks, H. B. Schlegel, G. E. Scuseria, M. A. Robb, J. R. Cheeseman, G. Scalmani, V. Barone, G. A. Petersson, H. Nakatsuji, M. C. X. Li, A. V. Marenich, J. Bloino, B. G. Janesko, R. Gompert, B. Mennucci, H. P. Hratchian, J. V. Ortiz, A. F. Izmaylov, J. L. Sonnenberg, D. Williams-Young, F. Ding, F. Lipparini, F. Egidi, J. Goings, B. Peng, A. Petrone, T. Henderson, D. Ranasinghe, V. G. Zakrzewski, J. Gao, N. Rega, G. Zheng, W. Liang, M. Hada, M. Ehara, K. Toyota, R. Fukuda, J. Hasegawa, M. Ishida, T. Nakajima, Y. Honda, O. Kitao, H. Nakai, T. Vreven, K. Throssell, J. J. A. Montgomery, J. E. Peralta, F. Ogliaro, M. J. Bearpark, J. J. Heyd, E. N. Brothers, K. N. Kudin, V. N. Staroverov, T. A. Keith, R. Kobayashi, J. Normand, K. Raghavachari, A. P. Rendell, J. C. Burant, S. S. Iyengar, J. Tomasi, M. Cossi, J. M. Millam, M. Klene, C. Adamo, R. Cammi, J. W. Ochterski, R. L. Martin, K. Morokuma, O. Farkas, J. B. Foresman and D. J. Fox, *Gaussian 16 Rev. B.01*, Gaussian Inc., Wallingford CT, 2016.
101 H. J. Werner, P. J. Knowles, G. Knizia, F. R. Manby and M. Schütz, Molpro: a general-purpose quantum chemistry program package, *Wiley Interdiscip. Rev.: Comput. Mol. Sci.*, 2012, **2**, 242–253.
102 H. J. Werner, P. J. Knowles, F. R. Manby, J. A. Black, K. Doll, A. Hesselmann, D. Kats, A. Köhn, T. Korona and D. A. Kreplin, The Molpro quantum chemistry package, *J. Chem. Phys.*, 2020, **152**, 144107.
103 H.-J. Werner, P. J. Knowles, P. Celani, W. Györffy, A. Hesselmann, D. Kats, G. Knizia, A. Köhn, T. Korona and D. Kreplin, *MOLPRO, a package of ab initio programs, version 1*, 2022.
104 J. Pople, J. Binkley and R. Seeger, *Int. J. Quantum Chem., Quantum Chem. Symp.*, 1976, **10**, 1–19.
105 K. Wohlever, Ohio Supercomputer Center Ohio Supercomputer 1087 Center, Columbus, OH, 1987.
106 S. Grimme, S. Ehrlich and L. Goerigk, *J. Comput. Chem.*, 2011, **32**, 1456–1465.
107 T. Yanai, D. Tew and N. Handy, A new hybrid exchange-correlation functional using the Coulomb-attenuating method (CAM-B3LYP), *Chem. Phys. Lett.*, 2004, **393**, 51–57.
108 A. D. Becke, New mixing of Hartree-Fock and local density-functional theories, *J. Chem. Phys.*, 1993, **98**, 1372.
109 J.-D. Chai and M. Head-Gordon, Long-range corrected hybrid density functionals with damped atom-atom dispersion corrections, *Phys. Chem. Chem. Phys.*, 2008, **10**, 6615–6620.
110 Y. Zhao and D. G. Truhlar, The M06 suite of density functionals for main group thermochemistry, thermochemical kinetics, noncovalent interactions, excited states, and transition elements: two new functionals and systematic testing of four M06-class functionals and 12 other functionals, *Theor. Chem. Acc.*, 2008, **120**, 215–241.
111 C. Adamo and V. Barone, Toward reliable density functional methods without adjustable parameters: The PBE0 model, *J. Chem. Phys.*, 1999, **110**, 6158–6169.
112 C. Møller and M. S. Plesset, *Phys. Rev.*, 1934, **46**, 618–622.
113 R. Krishnan and J. A. Pople, *Int. J. Quantum Chem.*, 1978, **14**, 91–100.
114 R. J. Bartlett and G. D. Purvis, *Int. J. Quantum Chem.*, 1978, **14**, 561–581.
115 T. Dunning, *J. Chem. Phys.*, 1989, **90**, 1007–1023.
116 D. Woon and T. Dunning, *J. Chem. Phys.*, 1995, **103**, 4572.
117 H. Hratchian and H. Schlegel, *Finding minima, transition states, and following reaction pathways on ab initio potential energy surfaces*, Elesvier, Amsterdam, 2005.
118 C. Peng and H. Bernhard Schlegel, *Isr. J. Chem.*, 1993, **33**, 449–454.
119 K. Fukui, *Acc. Chem. Res.*, 1981, **14**, 363–368.
120 R. J. Bartlett, Many-body perturbation theory and coupled cluster theory for electron correlation in molecules, *Annu. Rev. Phys. Chem.*, 1981, **32**, 359–401.
121 G. D. Purvis III and R. J. Bartlett, A full coupled-cluster singles and doubles model: The inclusion of disconnected triples, *J. Chem. Phys.*, 1982, **76**, 1910.
122 K. Raghavachari, G. W. Trucks, J. A. Pople and M. Head-Gordon, A fifth-order perturbation comparison of electron correlation theories, *Chem. Phys. Lett.*, 1989, **157**, 479–483.
123 B. Besler, J. K. Merz and P. Kollman, *J. Comput. Chem.*, 1990, **11**, 431–439.
124 E. D. Glendening, A. E. Reed, J. E. Carpenter and F. Weinhold, *NBO, NBO Version3.1*.
125 A. E. Reed, R. B. Weinstock and F. Weinhold, *J. Chem. Phys.*, 1985, **83**, 735–746.
126 R. Dennington, T. Keith and J. Millam, *GaussView, version 6.0. 16*, Semichem Inc., Shawnee Mission, KS, 2016, vol. 16.